

Wavelength multicasting in silicon photonic nanowires

Aleksandr Biberman,^{1,*} Benjamin G. Lee,¹ Amy C. Turner-Foster,² Mark A. Foster,³
Michal Lipson,³ Alexander L. Gaeta,³ and Keren Bergman¹

¹Department of Electrical Engineering, Columbia University, New York, New York, USA

²School of Electrical and Computer Engineering, Cornell University, Ithaca, New York, USA

³School of Applied and Engineering Physics, Cornell University, Ithaca, New York, USA

*biberman@ee.columbia.edu

Abstract: We demonstrate a scalable, energy-efficient, and pragmatic method for high-bandwidth wavelength multicasting using FWM in silicon photonic nanowires. We experimentally validate up to a sixteen-way multicast of 40-Gb/s NRZ data using spectral and temporal responses, and evaluate the resulting data integrity degradation using BER measurements and power penalty performance metrics. We further examine the impact of this wavelength multicasting scalability on conversion efficiency. Finally, we experimentally evaluate up to a three-way multicast of 160-Gb/s pulsed-RZ data using spectral and temporal responses, representing the first on-chip wavelength multicasting of pulsed-RZ data.

©2010 Optical Society of America

OCIS codes: (130.7405) Wavelength conversion devices; (190.4380) Nonlinear optics, four-wave mixing; (190.4390) Nonlinear optics, integrated optics; (230.4320) Nonlinear optical devices; (060.1155) All-optical networks; (060.4255) Networks, multicast.

References and links

1. M. Saruwatari, "All-optical signal processing for terabit/second optical transmission," *IEEE Sel. Top. Quantum Electron.* **6**(6), 1363–1374 (2000).
2. R. K. Pankaj, "Wavelength requirements for multicasting in all-optical networks," *IEEE/ACM Trans. Networking* **7**(3), 414–424 (1999).
3. H. Rong, R. Jones, A. Liu, O. Cohen, D. Hak, A. Fang, and M. Paniccia, "A continuous-wave Raman silicon laser," *Nature* **433**(7027), 725–728 (2005).
4. R. Claps, D. Dimitropoulos, V. Raghunathan, Y. Han, and B. Jalali, "Observation of stimulated Raman amplification in silicon waveguides," *Opt. Express* **11**(15), 1731–1739 (2003).
5. M. Dinu, F. Quochi, and H. Garcia, "Third-order nonlinearities in silicon at telecom wavelengths," *Appl. Phys. Lett.* **82**(18), 2954–2956 (2003).
6. H. K. Tsang, C. S. Wong, T. K. Liang, I. E. Day, S. W. Roberts, A. Harpin, J. Drake, and M. Asghari, "Optical dispersion, two-photon absorption and self-phase modulation in silicon waveguides at 1.5 μm wavelength," *Appl. Phys. Lett.* **80**(3), 416–418 (2002).
7. V. R. Almeida, C. A. Barrios, R. R. Panepucci, and M. Lipson, "All-optical control of light on a silicon chip," *Nature* **431**(7012), 1081–1084 (2004).
8. E. Dulkeith, Y. A. Vlasov, X. Chen, N. C. Panoiu, and R. M. Osgood, Jr., "Self-phase-modulation in submicron silicon-on-insulator photonic wires," *Opt. Express* **14**(12), 5524–5534 (2006).
9. I.-W. Hsieh, X. Chen, J. I. Dadap, N. C. Panoiu, R. M. Osgood, Jr., S. J. McNab, and Y. A. Vlasov, "Cross-phase modulation-induced spectral and temporal effects on co-propagating femtosecond pulses in silicon photonic wires," *Opt. Express* **15**(3), 1135–1146 (2007).
10. A. C. Turner-Foster, M. A. Foster, R. Salem, A. L. Gaeta, and M. Lipson, "Frequency conversion over two-thirds of an octave in silicon nanowaveguides," *Opt. Express* **18**(3), 1904–1908 (2010).
11. M. A. Foster, R. Salem, Y. Okawachi, A. C. Turner-Foster, M. Lipson, and A. L. Gaeta, "Ultrafast waveform compression using a time-domain telescope," *Nat. Photonics* **3**(10), 581–585 (2009).
12. Y. Dai, Y. Okawachi, A. C. Turner-Foster, M. Lipson, A. L. Gaeta, and C. Xu, "Ultralong continuously tunable parametric delays via a cascading discrete stage," *Opt. Express* **18**(1), 333–339 (2010).
13. A. C. Turner, M. A. Foster, A. L. Gaeta, and M. Lipson, "Ultra-low power parametric frequency conversion in a silicon microring resonator," *Opt. Express* **16**(7), 4881–4887 (2008).
14. M. A. Foster, A. C. Turner, R. Salem, M. Lipson, and A. L. Gaeta, "Broad-band continuous-wave parametric wavelength conversion in silicon nanowaveguides," *Opt. Express* **15**(20), 12949–12958 (2007).
15. R. Salem, M. A. Foster, A. C. Turner, D. F. Geraghty, M. Lipson, and A. L. Gaeta, "Signal regeneration using low-power four-wave mixing on silicon chip," *Nat. Photonics* **2**(1), 35–38 (2008).

16. M. A. Foster, A. C. Turner, J. E. Sharping, B. S. Schmidt, M. Lipson, and A. L. Gaeta, "Broad-band optical parametric gain on a silicon photonic chip," *Nature* **441**(7096), 960–963 (2006).
17. Q. Lin, J. Zhang, P. M. Fauchet, and G. P. Agrawal, "Ultrabroadband parametric generation and wavelength conversion in silicon waveguides," *Opt. Express* **14**(11), 4786–4799 (2006).
18. R. L. Espinola, J. I. Dadap, R. M. Osgood, Jr., S. J. McNab, and Y. A. Vlasov, "C-band wavelength conversion in silicon photonic wire waveguides," *Opt. Express* **13**(11), 4341–4349 (2005).
19. B. G. Lee, A. Biberman, N. Ophir, A. C. Turner-Foster, M. A. Foster, M. Lipson, A. L. Gaeta, and K. Bergman, "160-Gb/s broadband wavelength conversion on chip using dispersion-engineered silicon waveguides," *Proc. Conference on Lasers and Electro-Optics (CLEO), CThBB1* (2009).
20. B. G. Lee, A. Biberman, A. C. Turner-Foster, M. A. Foster, M. Lipson, A. L. Gaeta, and K. Bergman, "Demonstration of broadband wavelength conversion at 40 Gb/s in silicon waveguides," *IEEE Photon. Technol. Lett.* **21**(3), 182–184 (2009).
21. B. G. Lee, A. Biberman, M. A. Foster, A. C. Turner, M. Lipson, A. L. Gaeta, and K. Bergman, "Bit-error-rate characterization of silicon four-wave-mixing wavelength converters at 10 and 40 Gb/s," *Proc. Conference on Lasers and Electro-Optics (CLEO), CPDB4* (2008).
22. A. Biberman, N. Ophir, B. G. Lee, A. C. Turner-Foster, M. A. Foster, N. Sherwood-Droz, C. B. Poitras, M. Lipson, A. L. Gaeta, and K. Bergman, "All-optical spatial multicasting using cascaded silicon photonic devices," *Proc. European Conference on Optical Communication (ECOC), P2.27* (2009).
23. A. Biberman, B. G. Lee, K. Bergman, A. C. Turner-Foster, M. Lipson, M. A. Foster, and A. L. Gaeta, "First demonstration of on-chip wavelength multicasting," *Proc. Optical Fiber Communication Conference (OFC), OTuI3* (2009).
24. A. C. Turner, C. Manolatu, B. S. Schmidt, M. Lipson, M. A. Foster, J. E. Sharping, and A. L. Gaeta, "Tailored anomalous group-velocity dispersion in silicon channel waveguides," *Opt. Express* **14**(10), 4357–4362 (2006).
25. E. Dulkeith, F. Xia, L. Schares, W. M. J. Green, and Y. A. Vlasov, "Group index and group velocity dispersion in silicon-on-insulator photonic wires," *Opt. Express* **14**(9), 3853–3863 (2006).
26. M. A. Foster, A. C. Turner, M. Lipson, and A. L. Gaeta, "Nonlinear optics in photonic nanowires," *Opt. Express* **16**(2), 1300–1320 (2008).
27. G. P. Agrawal, *Nonlinear Fiber Optics* 3rd edn (Academic Press, San Diego, 2001).
28. J. L. Pleumeekers, J. Leuthold, M. Kauer, P. G. Bernasconi, C. A. Burrus, M. Cappuzzo, E. Chen, L. Gomez, and E. Laskowski, "All-optical wavelength conversion and broadcasting to eight separate channels by a single semiconductor optical amplifier delay interferometer," *Proc. Optical Fiber Communication Conference (OFC), ThDD4* (2002).
29. L. Rau, S. Rangarajan, D. J. Blumenthal, H.-F. Chou, Y.-J. Chiu, and J. E. Bowers, "Two-hop all-optical label swapping with variable length 80 Gb/s packets and 10 Gb/s labels using nonlinear fiber wavelength converters, unicast/multicast output and a single EAM for 80- to 10 Gb/s packet demultiplexing," *Proc. Optical Fiber Communication Conference (OFC), FD2-1–FD2-3* (2002).
30. C.-S. Brès, N. Alic, E. Myslivets, and S. Radic, "Scalable multicasting in one-pump parametric amplifier," *J. Lightwave Technol.* **27**(3), 356–363 (2009).
31. C.-S. Brès, A. O. J. Wiberg, B. P.-P. Kuo, N. Alic, and S. Radic, "Wavelength multicasting of 320-Gb/s channel in self-seeded parametric amplifier," *IEEE Photon. Technol. Lett.* **21**(14), 1002–1004 (2009).

1. Introduction

As the demand for bandwidth of optical networks continues to increase rapidly, spectral and temporal techniques for multiplexing are employed to increase data transmission capacity beyond terabit-per-second rates [1]. Communication between access networks is therefore densely aggregated, increasingly shifting performance emphasis toward core networks. This paradigm is independent of the communication platform, and prevails in telecommunication networks, data center interconnection networks, and networks-on-chip (NoCs). These high-bandwidth core networks may benefit from wavelength multicasting to simultaneously disperse information across multiple wavelength channels [2]. This indispensable functionality is traditionally performed in the electrical domain using power-hungry transceivers and electrical multiplexers/demultiplexers that do not scale well with data rate and number of wavelength channels. In this work, we demonstrate a scalable, energy-efficient, and pragmatic method for high-bandwidth wavelength multicasting using four-wave mixing (FWM) in silicon photonic nanowires. We evaluate the scalability of this technique for use within high-performance systems capitalizing on both spectral and temporal parallelism.

Photonic nanowires based on the highly-developed fabrication and processing of the complementary metal-oxide-semiconductor (CMOS)-compatible silicon-on-insulator (SOI) platform offer a novel domain for nonlinear optics. Inherently large nonlinear response and high optical confinement enabled by large refractive-index contrast allow for an enhancement of nonlinear interaction in these nanowires, translating to shorter interaction lengths and

compact devices for dense integration. Nonlinear silicon photonic devices based on the Raman effect [3,4], Kerr effect [5,6], two-photon absorption (TPA) [5,6], and free-carrier dispersion (FCD) [4,7] have all been demonstrated.

Sufficient nonlinear interaction in silicon photonic nanowires gives rise to parametric processes based on self-phase modulation [6,8], cross-phase modulation [9], and FWM [10–18]. Leveraging these parametric processes, parametric systems such as all-optical modulators and switches [7], regenerators [15], amplifiers [3,4,16], tunable delays [12], pulse compressors [11], wavelength converters [10,13,17–21], and wavelength multicasters [22,23] have all been demonstrated. Dispersion engineering, the tailoring of group-velocity dispersion (GVD) of silicon photonic nanowires, is critical for high-bandwidth operation of parametric processes [10,24,25]. In this platform, the dominant dispersion is dictated by waveguide dispersion, which allows for the engineering of the total GVD with tuning of the nanowire dimensions [24–26]. These devices enable ultra-broadband FWM operation. Wavelength conversion across over 830 nm has already been demonstrated in this platform [10].

2. Wavelength conversion and wavelength multicasting

Wavelength conversion using degenerate FWM is achieved by combining a continuous-wave (CW) pump with a modulated signal. Some of the energy from the pump is converted to both amplify the original signal and also create a new modulated idler [27]. The wavelength-converted data of the idler is identical to the original signal data. Our previous work with dispersion-engineered silicon photonic nanowires leveraged FWM to perform first bit-error rate (BER) characterization of wavelength-converted data, demonstrating error-free (defined as having BERs less than 10^{-12}) wavelength conversion of 10- and 40-Gb/s non-return-to-zero (NRZ) data, across 35 and 12 nm, respectively [21]. We then demonstrated wavelength conversion of 40-Gb/s NRZ data across 47.7 nm [20]. To verify the feasibility of this device within a pulsed-return-to-zero (RZ) environment, we then demonstrated wavelength conversion of 160-Gb/s time-division-multiplexed data across 21 nm, representing the first pulsed-RZ wavelength conversion using this integrated platform [19].

In this work, the method for achieving wavelength multicasting using FWM combines an amplitude-modulated pump with multiple CW signals, producing multiple wavelength-multicasted modulated idlers encoded with data identical to the pump data. Previous efforts demonstrating wavelength multicasting leveraged parametric processes in semiconductor optical amplifiers (SOAs) [28], dispersion-shifted fiber (DSF) [29], and highly-nonlinear fiber (HNLF) [30]. Using HNLF, another wavelength multicasting technique was demonstrated with self-seeded pumps [31]. Using dispersion-engineered silicon photonic nanowires, we have shown the first wavelength multicasting in a CMOS-compatible integrated platform, demonstrating up to an eight-way error-free multicast of 40-Gb/s NRZ data [23]. Using BER characterization, we observed no increase in power penalty (the degradation in receiver sensitivity incurred by the device) when scaling from a one-way to an eight-way multicast, demonstrating the potential for further scalability. The conversion efficiency, defined as the difference in the peak power between the input signals and output idlers (both at the output of the chip), remained constant for each wavelength multicasting configuration, confirming the scalability potential [23]. We further demonstrated this method in a wavelength-routing environment, utilizing wavelength multicasting in silicon photonic nanowires and wavelength demultiplexing using silicon photonic microring resonator-based filters to route each multicasted wavelength channel to its respective destination [22]. Error-free operation of this spatial multicasting functionality was demonstrated with up to a three-way multicast of 10-Gb/s NRZ data [22].

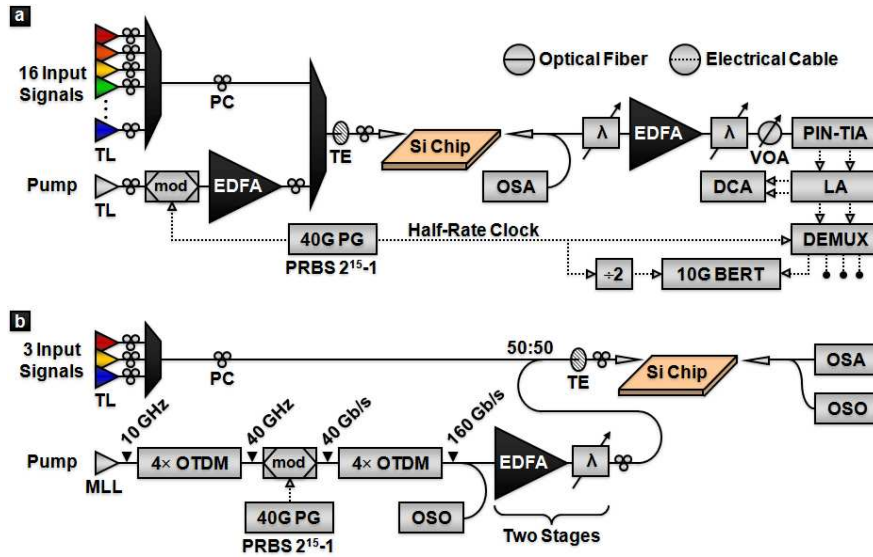


Fig. 1. Experimental setup diagrams for wavelength multicasting using the silicon photonic nanowire. (a) Experimental setup for up to a sixteen-way multicast of 40-Gb/s NRZ data. (b) Experimental setup for up to a three-way multicast of 160-Gb/s pulsed-RZ data. In this work, wavelength multicasting using FWM is achieved with an amplitude-modulated pump combined with multiple CW input signals, producing multiple wavelength-multicast modulated output idlers encoded with data identical to the pump data.

3. Experimental setup

The device discussed here is a 1.1-cm-long dispersion-engineered silicon photonic nanowire with a height of 290 nm, slab thickness of 25 nm, and width of 660 nm. It was fabricated using electron-beam lithography followed by reactive-ion etching. The experimental setup for BER measurements conducted for the wavelength multicasting of 40-Gb/s NRZ data incorporates sixteen multiplexed CW tunable laser (TL) sources (occupying wavelength channels C21 through C36 within the ITU grid) acting as input signals, and another TL source as the pump [Fig. 1(a)]. The pump is externally modulated with a 40-Gb/s NRZ on-off-keyed (OOK) signal, encoded using a pseudo-random bit sequence (PRBS) of length $2^{15}-1$, generated by a pattern generator (PG). The pump is amplified using an erbium-doped fiber amplifier (EDFA) and then combined with the input signals using a dense wavelength-division multiplexer (DWDM). The combined signals then pass through a fiber polarizer, selecting the transverse-electric (TE) polarization, before being coupled into the on-chip nanotapered waveguide through a tapered fiber. After exiting the chip, the optical streams pass through a tunable grating filter (λ), selecting the proper wavelength-multicast output idler to evaluate, an EDFA, another tunable grating filter, and a variable optical attenuator (VOA). The selected output idler is then received by a high-speed PIN photodiode and transimpedance amplifier (PIN-TIA) receiver followed by a limiting amplifier (LA). Using an electrical demultiplexer (DEMUX), the received 40-Gb/s data is then spatially demultiplexed into four 10-Gb/s electrical data streams, all of which are verified for uniformity, and one of which is evaluated using a 10-Gb/s BER tester (BERT). Both the DEMUX and the BERT are synchronized to the clock output of the PG. A power tap is inserted before the first filter for examination on an optical spectrum analyzer (OSA) with a 0.06-nm resolution bandwidth, and a digital communications analyzer (DCA) is used to verify the electrical data stream following the LA. Polarization controllers (PCs) are also used throughout the setup. Before insertion, the average pump power is 24 dBm, and the input signals are each set to -2 dBm. The fiber-to-fiber coupling loss with the pump and input signals passing into the chip is 11.7 dB.

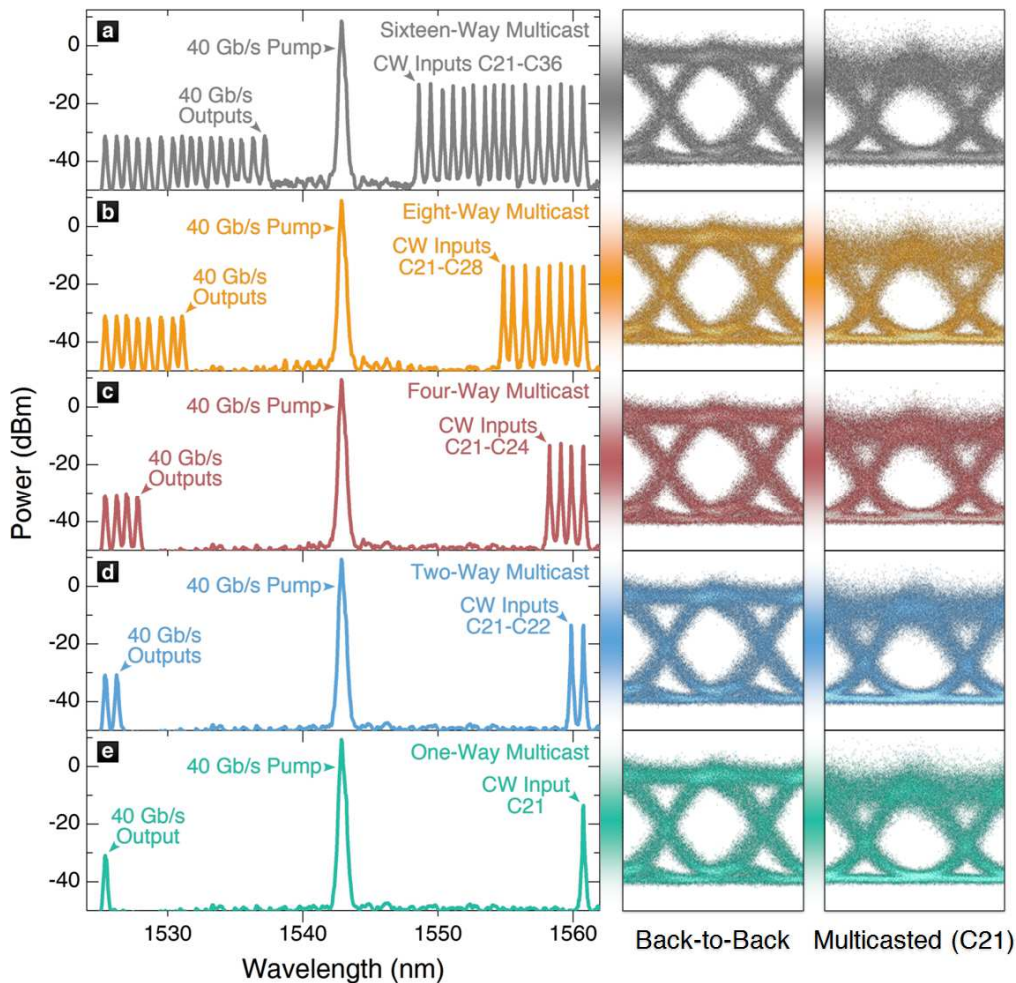


Fig. 2. Experimentally-measured spectral and temporal responses for up to a sixteen-way multicast of 40-Gb/s NRZ data. Output spectra (with a 0.06-nm resolution bandwidth) and eye diagrams (with a 50-ps temporal window) for the wavelength multicasting configurations and back-to-back configuration of the (a) sixteen-way, (b) eight-way, (c) four-way, (d) two-way, and (e) one-way multicast. The wavelength-multicasted eye diagrams correspond to the wavelength-multicasted wavelength channel C21 within the ITU grid, which is wavelength multicasted in every configuration and has the largest conversion bandwidth of 35.8 nm. The back-to-back eye diagram is recorded for the pump bypassing the silicon photonic chip with all the input signals off, replacing the chip with a VOA set to mimic the fiber-to-fiber insertion loss through the chip. The conversion efficiency remains constant at -15.2 dB for each wavelength multicasting configuration.

The experimental setup for measurements conducted for wavelength multicasting of 160-Gb/s pulsed-RZ data incorporates three multiplexed CW TL sources (occupying wavelength channels C21, C27, and C33 within the ITU grid) acting as input signals, and another TL source as the pump [Fig. 1(b)]. The pump incorporates a 10-GHz mode-locked fiber laser (MLL) with a 1.5-ps pulse width, and a fourfold optical time-division multiplexer ($4 \times$ OTDM) to generate a 40-GHz pulse train, which is then externally modulated with a 40-Gb/s pulsed-RZ OOK signal, encoded using a PRBS of length $2^{15}-1$, by the PG. The optical stream then travels through another $4 \times$ OTDM, generating a 160-Gb/s pump, which is then amplified using two stages, each consisting of an EDFA and a tunable grating filter. The 160-Gb/s pump is then combined with the input signals using a 3-dB coupler, and the combined optical streams then pass through a fiber polarizer, selecting the TE polarization, before being

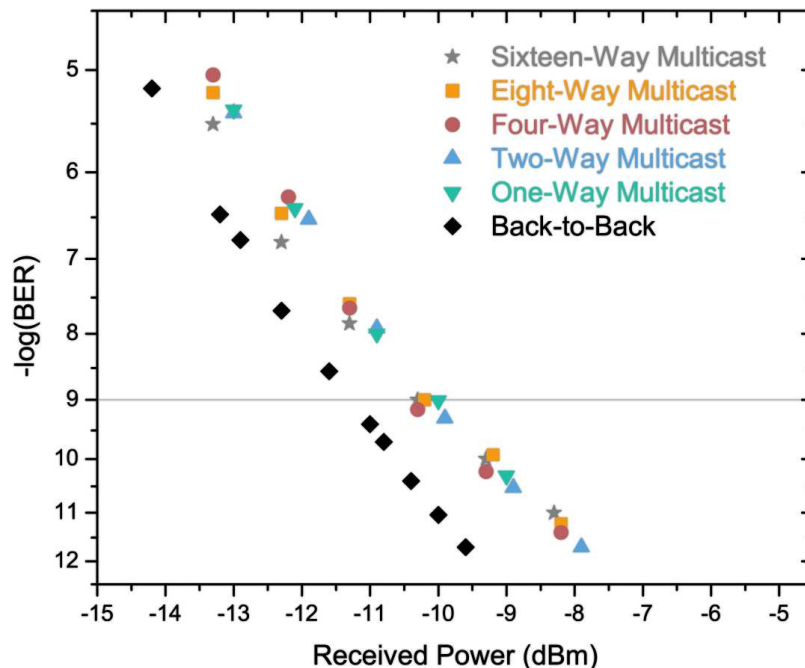


Fig. 3. Experimentally-measured BER curves for up to a sixteen-way multicast of 40-Gb/s NRZ data. BER curves for the wavelength multicasting configurations and back-to-back configuration of the sixteen-, eight-, four-, two-, and one-way multicast. The wavelength-multicasted BER curves correspond to the wavelength-multicasted wavelength channel C21 within the ITU grid, which is wavelength multicasted in every configuration and has the largest conversion bandwidth of 35.8 nm. Error-free wavelength multicasting operation is observed for all configurations. The back-to-back BER curve is recorded for the pump bypassing the silicon photonic chip with all the input signals off, replacing the chip with a VOA set to mimic the fiber-to-fiber insertion loss through the chip, producing a constant 1.3-dB power penalty for up to the sixteen-way multicast of 40-Gb/s NRZ data.

coupled into the on-chip nanotapered waveguide through a tapered fiber. After exiting the chip, the spectral response of the optical streams is examined using an OSA, and the temporal response is examined using an optical sampling oscilloscope (OSO). The OSO is also used to examine the temporal response of the generated optical stream after the OTDM stages. PCs are also used throughout the setup. Before insertion, the average pump power is 21 dBm, and the input signals are each set to 2.4 dBm. Here, the fiber-to-fiber coupling loss with the pump and input signals passing into the chip is 9.1 dB.

4. Experimental validation

We first perform up to a sixteen-way multicast of 40-Gb/s NRZ data using the experimental setup depicted in Fig. 1(a) and described in the experimental setup section. Sixteen CW input signals, each placed on a wavelength channel within the ITU grid (across C21–C36) with a 100-GHz separation, are combined with a pump modulated with 40-Gb/s NRZ data, and are passed through the nanowire. The resulting interaction produces sixteen multicasted output idlers, each encoded with the 40-Gb/s NRZ data [Fig. 2(a)]. The input signals span 12.5 nm (1548.5 nm to 1561.0 nm), the pump is placed at the 1543.0-nm wavelength, and the wavelength-multicasted output idlers span 12.2 nm (1525.2 nm to 1537.4 nm), producing a conversion bandwidth ranging from 11.1 nm to 35.8 nm. An eight-way multicast is then achieved by turning off eight CW input signals, leaving C21–C28 [Fig. 2(b)]. A four-way multicast is similarly achieved by consequently turning off four more input signals, leaving C21–C24 [Fig. 2(c)]. Similarly, a two-way [Fig. 2(d)] and a one-way [Fig. 2(e)] multicast is achieved by turning off two input signals (leaving C21–C22) and one input signal (leaving

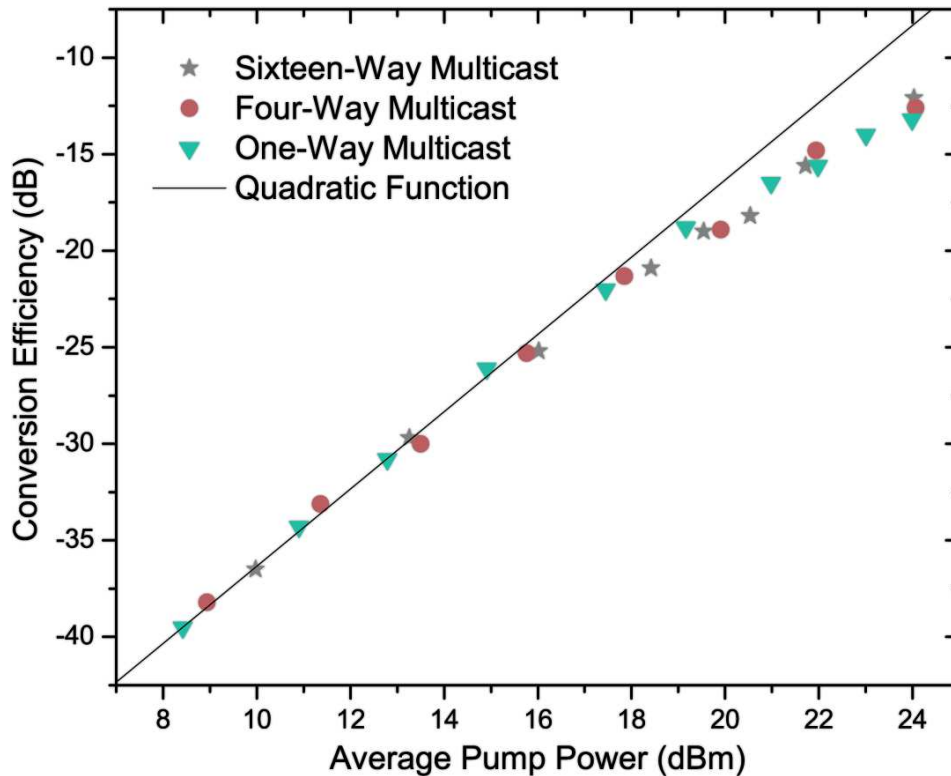


Fig. 4. Experimentally-measured dependence of conversion efficiency on average pump power for up to a sixteen-way multicast. The relationship between conversion efficiency and average pump power injected into the silicon photonic nanowire is evaluated for the wavelength multicasting configurations of the sixteen-, four-, and one-way multicast. All configurations exhibit a quadratic relationship between conversion efficiency and average pump power, displaying saturation at peak (average) powers above 21 (18) dBm. The overlapping curves indicate no adverse effects on this relationship from scaling up to the sixteen-way multicast.

C21), respectively. The conversion efficiency remains constant at -15.2 dB for each wavelength multicasting configuration [Fig. 2(a)–2(e)]. Furthermore, we observe the same constant conversion efficiency for other arbitrary wavelength multicasting configurations, with arbitrary permutations of the sixteen input signals. These results confirm and surrogate the wavelength multicasting scalability demonstrated in our previous work [22,23].

In our previous work, we have experimentally measured a constant 6.8-dB power penalty for up to an eight-way multicast of 40-Gb/s NRZ data, where the back-to-back BER curve was recorded for the pump directly at the output of the silicon photonic chip [23]. In this work, the back-to-back BER curve is recorded for the pump bypassing the chip, replacing the chip with a VOA set to mimic the fiber-to-fiber insertion loss through the chip. Here, the pump travels through the same experimental path as the wavelength-multicast signals, including filtering and amplification stages. The filtering stages suppress out-of-band amplified spontaneous emission (ASE) noise generated by the pump EDFA, improving the back-to-back BER curve. Furthermore, using a preamplifier EDFA with a lower sensitivity threshold and noise figure, we also improve the BER curves of the wavelength-multicast signals. The resulting experimentally-measured constant 1.3-dB power penalty in this work represents much improvement over our previous work.

For all the aforementioned configurations, the data integrity degradation experienced by the wavelength multicasting process is evaluated and quantified using experimentally-obtained eye diagrams and BER characterization. First, similar open eye diagrams are observed for each wavelength-multicast wavelength channel, and recorded (with a 50-ps

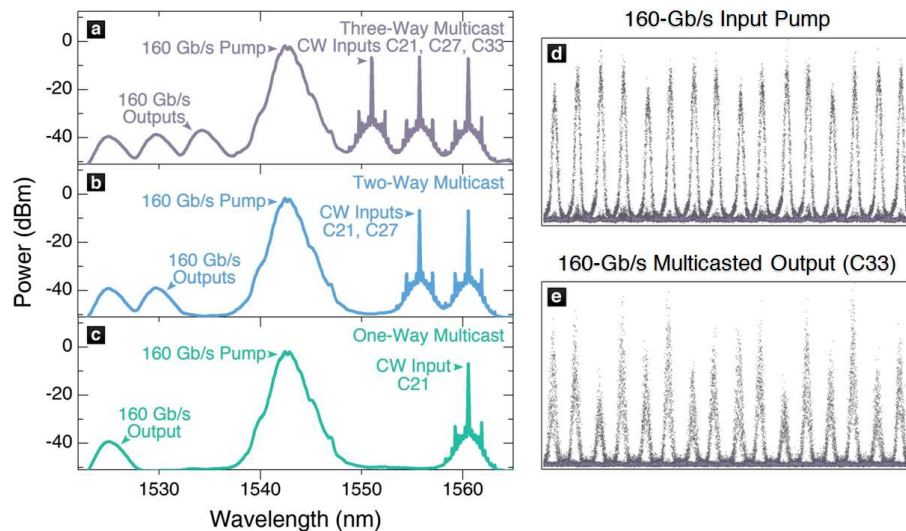


Fig. 5. Experimentally-measured spectral response for up to a three-way multicast of 160-Gb/s pulsed-RZ data, as well as temporal response for the generated and wavelength-multicast optical data. Output spectra (with a 0.06-nm resolution bandwidth) for the wavelength multicasting configurations of the (a) three-way, (b) two-way, and (c) one-way multicast. The demonstrated conversion bandwidth reaches up to 36.8 nm. The conversion efficiency remains constant at -22.8 dB for each wavelength multicasting configuration. The measured optical signal-to-noise ratio (OSNR) in the spectra is limited by the dynamic range of the OSA. Eye diagrams (with a 100-ps temporal window) of 160-Gb/s pulsed-RZ data for the (d) generated optical data and (e) wavelength-multicast wavelength channel C33 within the ITU grid, during a three-way multicast.

temporal window) for wavelength-multicast wavelength channel C21, which is wavelength multicasted in every configuration and has the largest conversion bandwidth [Fig. 2(a)–2(e)]. These eye diagrams are compared with the back-to-back case eye diagram, which is recorded for the pump bypassing the silicon photonic chip with all the input signals off, replacing the chip with a VOA set to mimic the fiber-to-fiber insertion loss through the chip [Fig. 2(a)–2(e)]; the pump travels through the same path as the wavelength-multicast signals. For the same wavelength-multicast wavelength channel, we observe error-free transmission using BER characterization for each configuration. We subsequently record a BER curve for each case (Fig. 3). All five wavelength multicasting cases produce overlapping BER curves, indicating no additional power penalty associated with scaling up to the sixteen-way multicast. Moreover, taking a BER curve for the back-to-back case produces a constant 1.3-dB power penalty for up to the sixteen-way multicast of 40-Gb/s NRZ data.

The conversion efficiency of wavelength conversion and wavelength multicasting has a dependence on the average pump power injected into the silicon photonic nanowire [15]. To quantify how this interaction is affected by the scalability of wavelength multicasting, we experimentally evaluate the dependence of conversion efficiency on average pump power for sixteen-, four-, and one-way multicast configurations (Fig. 4). For all configurations, we obtain a quadratic relationship between conversion efficiency and average pump power, displaying saturation at peak (average) powers above 21 (18) dBm due to TPA-induced free-carrier absorption (FCA) [15]. Moreover, the curves overlap, indicating no adverse effects on this relationship from scaling up to a sixteen-way multicast (Fig. 4).

To demonstrate the practicality of using this wavelength multicasting method in a time-division-multiplexed pulsed-RZ environment, we demonstrate up to three-way multicast of 160-Gb/s pulsed-RZ data, using the experimental setup depicted in Fig. 1(b) and described in the experimental setup section. Here, three CW input signals, each placed on a wavelength channel within the ITU grid (corresponding to C21, C27, and C33) with a 600-GHz separation, are combined with a pump encoded with 160-Gb/s pulsed-RZ data. The resulting

interaction in the silicon photonic nanowire produces three wavelength-multicast output idlers, each encoded with the 160-Gb/s pulsed-RZ data [Fig. 5(a)]. Here, the input signals span 9.9 nm (1550.9 nm to 1560.8 nm), the pump is placed at the 1542.7-nm wavelength, and the wavelength-multicast output idlers span 11.4 nm (1524.0 nm to 1535.4 nm), producing a conversion bandwidth ranging from 15.5 nm to 36.8 nm. Similarly, a two-way [Fig. 5(b)] and one-way [Fig. 5(c)] multicast is achieved by turning off two input signals (leaving C21 and C27) and one input signal (leaving C21), respectively. The conversion efficiency remains constant at -22.8 dB for each wavelength multicasting configuration. We further examine the temporal properties of the generated optical pulses [Fig. 5(d)], as well as the wavelength-multicast optical pulses for wavelength channel C33 in the three-way multicast configuration [Fig. 5(e)]. The eye diagram (with a 100-ps temporal window) of the wavelength-multicast pulsed-RZ data remains open during the three-way multicasting operation. After the OTDM stages, the amplitudes of the individual tributaries of the signal are not perfectly uniform due to asymmetrical insertion losses within each OTDM stage [Fig. 5(d)]; this is exacerbated by wavelength multicasting due to the quadratic relationship between conversion efficiency and pump power [Fig. 5(e)]. The tributary uniformity can be improved by further normalizing the insertion losses in each OTDM stage. To the best of our knowledge, this work represents the first on-chip wavelength multicasting demonstration using pulsed-RZ data.

5. Conclusion

We have shown and evaluated an efficient and scalable method of wavelength multicasting high-speed optical streams encoded with both 40-Gb/s NRZ data and 160-Gb/s pulsed-RZ data. We have verified up to a sixteen-way multicast of 40-Gb/s NRZ data using spectral and temporal responses, and quantified the resulting wavelength-multicast data integrity degradation using BER and power penalty performance metrics. We then evaluated the effect of this wavelength multicasting scalability on the dependence of conversion efficiency on average pump power. We further evaluated spectrally and temporally up to a three-way multicast of 160-Gb/s pulsed-RZ data. Every quantifiable experimentally-verified metric that we examined suggests that this method for wavelength multicasting is a truly scalable process. The massive bandwidth offered by this dispersion-engineered silicon photonic nanowire, combined with the platform's CMOS compatibility and capability of ultra-dense integration with complex photonics and electronics, materializes this wavelength multicasting method for full-scale parametric systems such as photonic routers-on-chip (RoCs) for ultra-broadband high-performance optical networks.

Acknowledgements

This work was supported in part by the Defense Advanced Research Projects Agency (DARPA) MTO Parametric Optical Processes and Systems program under contract number W911NF-08-1-0058. This work was performed in part at the Cornell NanoScale Facility, a member of the National Nanotechnology Infrastructure Network, which is supported by the National Science Foundation.